AIAA JOURNAL
Vol. 30, No. 5, May 1992

Multifractal Analysis of a Lobed Mixer Flowfield Utilizing the Proper Orthogonal Decomposition

L. Ukeiley,* M. Varghese,† M. Glauser,‡ and D. Valentine§
Clarkson University, Potsdam, New York 13699

We use the theory of multifractal measures to throw a fresh perspective on the data analysis of velocity time traces in a lobed mixer flow. A lobed mixer is a device that enhances mixing through secondary flows and streamwise vorticity. A specially designed rake of hot wires with high spatial resolution was used to collect the streamwise velocity data. Through the use of the proper orthogonal decomposition, a basic knowledge of the coherent structures, on an energy weighted basis, was studied. The instantaneous velocity traces that are necessary for calculating the generalized fractal dimensions are reproduced from the ensemble average measurements taken from the proper orthogonal decomposition. We compute the generalized fractal dimensions D_q and the $f(\alpha)$ multifractal spectrum of several proper eigenmodes for data samples from the velocity time trace of several hot-wire probes at different energy levels. This is a marked departure from previous multifractal theory applications to self-similar cascades that mainly dealt with the dissipation fields of turbulent kinetic energy. In the course of this exposition it will be pointed out that in certain cases a single dimension D_1 may suffice to capture the entire spectrum of scaling exponents for the velocity time trace. We verify that in such cases the location of the hot-wire probes imply a lack of intermittency.

Nomenclature

a_n	= random coefficient
D	= Hausdorff or single fractal dimension
D_q	= generalized fractal dimension
$f(\alpha)$	= multifractal singularity spectrum
N_δ	= smallest number of bins needed to cover the data
p_i	= invariant probability density function
q	= moment of the invariant probability density function
R_{ij}	= cross-correlation tensor
$S(x,f)$	= streamwise energy power spectrum
u	= velocity vector field
u_1	= instantaneous streamwise velocity
$\hat{u}_1$	= Fourier transform of streamwise velocity
x	= horizontal direction across lobes
y	= vertical distance across lobes
$\bar{y}$	= vertical location of rake for data collection
z	= streamwise direction
$\bar{z}$	= streamwise location of rake for data collection
α	= singularity measure
δ	= bin width for calculating fractal dimension
$\lambda(f)$	= eigenspectra of streamwise turbulent kinetic energy
μ	= intermittency exponent
Φ_{ij}	= cross-spectral tensor
ϕ_i	= eigenvector
ψ_i	= eigenvector in transform domain

Introduction

WE use multifractal measures in conjunction with the proper orthogonal decomposition (POD) to study streamwise velocity time traces in the downstream region of a lobed mixer flow. A lobed mixer is essentially a forced mixer that induces rapid mixing by enhancing streamwise vorticity (see Fig. 1). This enhanced mixing is accomplished with relatively low total pressure loss. Low pressure loss has made these devices desirable for many uses. One example is in turbofan engines where they are used to reduce noise levels by efficiently mixing cool bypass air with the hot engine exhaust air.

Lobed forced mixers similar to the one used in this study have been examined in several experiments. Paterson[1] collected the first detailed experimental data in the flowfield downstream of a lobed mixer. His studies showed that there were strong secondary flows along with streamwise vortices about the scale of the lobe height. The formation of the streamwise vorticity was attributed to inviscid effects. Werle et al.[2] studied the downstream region with the use of dye injection in a water tunnel. Their results defined three distinct regions of vortex development along with backing Paterson's results that the vortices were formed through inviscid effects. Eckerle et al.[3] conducted an experimental study in the downstream region of a lobed mixer using single-point laser

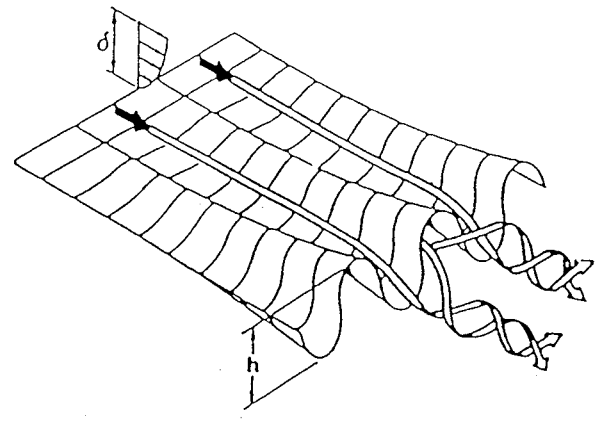

Fig. 1 Lobed mixer enhancing streamwise vorticity, from Werle et al.[2]

Presented as Paper 91-0521 at the AIAA 29th Aerospace Sciences Meeting, Reno, NV, Jan. 7–10, 1991; received Jan. 21, 1991; revision received July 26, 1991; accepted for publication July 28, 1991.

*Graduate Research Assistant, Department of Mechanical and Aeronautical Engineering. Student Member AIAA.

†Assistant Professor, Department of Electrical and Computer Engineering; currently Assistant Professor, Engineering, Harvey Mudd College, Claremont, CA 91711.

‡Assistant Professor, Department of Mechanical and Aeronautical Engineering. Member AIAA.

§Associate Professor, Department of Mechanical and Aeronautical Engineering.

Doppler anemometer measurements. Their results showed the three regions defined by Werle et al.[2] and determined that, by varying the velocity ratio across the lobe, the location of these regions could be shifted. It was concluded from their data that the streamwise vortices escaped from the boundary layers of the plate, thus indicating that viscous effects are important in the development of these vortices. Lasheras and Meiburg[4] conducted experiments to study where and how the streamwise vortices were formed. They found counter-rotating streamwise vortex tubes located in the braids of connecting Karman vortices in the shear layer downstream of a sinusoidally perturbed flat plate (similar to the lobed mixer studies here).

Lumley[5] developed the POD technique to objectively identify the coherent structure or large eddy in a turbulent flow. The method was first applied to the wake behind a cylinder by Payne.[7] The results of this study showed that the energy content in, what was defined to be, the dominant eddy was not significantly larger than that in subsequent eddies. Bakewell and Lumley[8] applied the technique on measurements taken in the near-wall region of turbulent pipe flow. These results were more conclusive than the previous experiment, showing the dominant eddy to contain 90% of the total streamwise turbulent energy. Moin[9] applied the POD to data generated by a large eddy simulation of a turbulent channel flow. His results showed that the dominant eddy contained up to 64% of the turbulent kinetic energy; Herzog[10] utilized the POD technique on hot-film anemometer measurements taken in the near-wall region of a turbulent boundary layer. The results obtained showed the dominant eigenmode to contain approximately 60% of the total kinetic energy; these results were consistent with the results obtained by Moin's simulation. Leib et al.,[11] Glauser et al.,[12] and Glauser and George[13] applied the POD to the near-field region of a turbulent axisymmetric jet. Their results showed that the first eigenmode contained approximately 40% of the total turbulent kinetic energy and that accurate representation of the flowfield can be obtained by using only the first three eigenmodes. Sirovich et al.[14] applied the decomposition technique to turbulent convection flow simulation for the case of stress-free boundary conditions. For their flow conditions, the first eigenmode contained 43% of the kinetic energy with 60% of energy being represented by the summation of the first five modes. Chambers et al.[15] utilized the POD to examine Monte Carlo simulations of a randomly forced Burgers' equation. They showed that the number of proper orthogonal modes needed to reproduce 90% of the total energy increased with energy. Delville et al.[16] applied the POD to the wake downstream of a flat plate, finding 70% of the mean-square streamwise velocity recovered within the first three modes. More recently, Sirovich et al.[17] and Winter et al.[18] applied the POD to digital images obtained in a turbulent jet and jets in crossflow, respectively. In the later study, the technique was used in an attempt to quantify how well the flow was mixed.

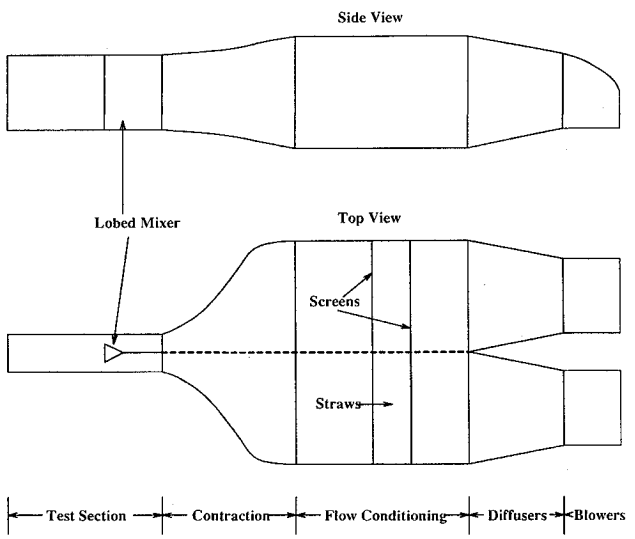

Fig. 2 Wind-tunnel schematic.

Kolomogorov[19] first proposed that the cascading process that governs the rate of dissipation, through the various scales of a turbulent flow, was statistically independent. He postulated that the logarithm of the rate of dissipation satisfied a Gaussian distribution. This was known as the log-normal model. This was superseded by Mandelbrot's work in 1972[20] that showed the limitations of Kolomogorov's third hypothesis and exposed the divergence of high moments of the dissipation field. Mandelbrot[21] used a fractal model for the dissipation and distinguished between absolute and weighted curdling. Weighted curdling turned out to be the first description of what is now commonly known as multifractal formalism in turbulence. Prasad et al.[31] have extensively studied the multifractal nature of the dissipative field using both the (D_q,q) and the $(f(\alpha),\alpha)$ methods. Meneveau and Sreenivasan[22] showed that (for several examples in fully developed turbulence) a simple two-scale Cantor set model seemed to fit the scaling exponents of the dissipation field.

In the current study, multipoint hot-wire measurements were taken in the downstream region of a lobed mixer flow. The POD technique was then applied in the spanwise direction using the streamwise velocity cross-correlation tensor. Contributions to velocity time traces were reproduced for various proper orthogonal modes and their contribution to the original signal studied. Both the (D_q,q) and the $(f(\alpha),\alpha)$ curves were computed for the reconstructed streamwise velocity time traces for the first three individual proper orthogonal modes. Large positive values of q for the (D_q,q) curve indicate the region where the measure is most singular. The value of D_q for large positive q therefore indicates regions with greater turbulence intensity in the flow field. The (D_q,q) is simpler to compute numerically and most researchers have used the Legendre transformations to obtain the $(f(\alpha),\alpha)$ curves from the (D_q,q) graphs. It has been pointed out that these methods smooth out significant characteristics of the $(f(\alpha),\alpha)$ curves especially if one were dealing with phase transitions. We use a method first described by Mandelbrot[23] and later developed by Chhabra and Jensen[24] to directly obtain the $(f(\alpha),\alpha)$ curves. The (D_q,q) curve is shown to have sufficient richness in its variation when the intermittency exponent $(-2dD_q/dq$ at $q=0)$ was high. In cases when the intermittency was small, it was found that the (D_q,q) curve flattened out at $q=1$. This implies that D_1 captures almost all the variations in the scaling exponents for these regions in the flow.

Proper Orthogonal Decomposition

Lumley[5] suggested the use of the POD technique in 1967, based on the Karhunen-Loeve expansion (see Ref. 6), in an attempt to objectively define coherent structures in turbulent flows. This theory has been used to predict the energy content and form of coherent structures. Lumley proposed that the coherent structure should be the structure with the largest mean-square projection on the random velocity field (i.e., maximization of energy). This is shown in the following equation where $\phi(x,t)$ is the candidate structure, $u(x,t)$ the instantaneous velocity, and β is the inner product of the two:

$$\overline{|u\cdot\phi|^2}=\overline{|\beta|^2} \tag{1}$$

Equation (1) is assumed to be normalized by the modulus of ϕ since it is the degree of the projection that is of interest not the amplitude.

Maximizing the mean-square projection leads to the following eigenvalue problem:

$$\int\int\int\int R_{ij}(x,x',t,t')\phi_j^{(n)}(x',t')\,dx'\,dt'=\lambda^{(n)}\phi_i^{(n)}(x,t) \tag{2}$$

where the kernel of Eq. (2) is the velocity cross-correlation tensor

$$R_{ij}(x,x',t,t') = \overline{u_i(x,t)u_j(x',t')}$$

and the eigenvalue is $\lambda = \overline{|\beta|^2}$. The previous equation has an infinite number of orthonormal solutions that can be used to reconstruct the original random signal from the following equation,

$$u_i(x,t) = \sum_{n=1}^{\infty} a_n \phi_i^{(n)}(x,t) \tag{3}$$

where the coefficients a_n are random and uncorrelated and are obtained from

$$a_n = \int u_i(x,t)\phi_i^{(n)}(x,t)\, dx \tag{4}$$

If a direction is assumed to be statistically stationary, the POD reduces to the more familiar harmonic decomposition so that Fourier analysis is sufficient in that direction. Under the conditions for the lobed mixer, Eq. (2) reduces to

$$\int\int\int \Phi_{ij}(x,x',y,y',z,z',f)\psi_j^n(x',y',z',f)\, dx'\, dy'\, dz'$$
$$= \lambda^{(n)}(f)\psi_i^n(x,y,z,f) \tag{5}$$

where $\Phi_{ij}(x,x',y,y',z,z',f)$ is the Fourier transform of $R_{ij}(x,x',t,t')$ in the stationary direction (i.e., time), the ψ are the frequency dependent eigenfunctions, and x, y, and z denote the inhomogeneous directions (see Fig. 4). It should be noted that the Fourier transform is only utilized in time, whereas the POD is used to supply the basis sets in the spatially inhomogeneous directions.

In this study, a simpler one-dimensional version of this decomposition, using one-dimensional cross spectra, obtained at one downstream and vertical location can be developed into the equation,

$$\int \Phi_{11}(x,x',\bar{y},\bar{z},f)\psi_1^{(n)}(x',\bar{y},\bar{z},f)\, dx' = \lambda^{(n)}(f)\psi_1^{(n)}(x,\bar{y},\bar{z},f) \tag{6}$$

where $\bar{y}$ and $\bar{z}$ denote the vertical and downstream locations where the measurements were obtained. In Eq. (6), only the spanwise direction x is decomposed through the use of POD. The vertical and streamwise directions are also statistically inhomogeneous in this flow, but are not considered in this initial study. For the remaining part of this discussion, $\bar{y}$ and $\bar{z}$ will be dropped because they are held constant at 28.5 and 100 mm, respectively (see Fig. 4). The streamwise velocity, which was decomposed through Fourier analysis (from time to frequency), can be reproduced in Fourier space by

$$\hat{u}_1(x,f) = \sum_{n=1}^{\infty} a_n(f)\psi_1^{(n)}(x,f) \tag{7}$$

where the random coefficients $a_n(f)$ can be calculated from

$$a_n(f) = \int \hat{u}_1(x,f)\psi_1^{(n)*}(x,f)\, dx \tag{8}$$

where the asterisk denotes complex conjugate. The streamwise velocity in Fourier space can then be inverse transformed to obtain the reproduced instantaneous velocity time trace. The energy spectrum can be reconstructed from

$$S(x,f) = \sum_{n=1}^{\infty} \lambda^{(n)}(f)\psi_1^{(n)}(x,f)\psi_1^{(n)*}(x,f) \tag{9}$$

where $\lambda^{(n)}(f)$ are the eigenspectra. The eigenspectra represent the streamwise turbulent kinetic energy integrated over the domain to which the POD is applied. The convergence of the eigenspectra and eigenvectors is dependent on the total amount of energy in the spectrum. It has been shown (Ref. 25) that if a different subdomain is chosen over which the POD is applied, then the rate of convergence can be varied. This is something that will be studied in this flow at a later date. The numerical approximation simply consists of replacing the integral in Eq. (6) by an appropriate quadrature rule (in this study a trapezoidal rule) and this is detailed by Glauser et al.[12] In brief then, $\Phi_{11}(x,x',\bar{y},\bar{z},f)$ is obtained from experimental measurements and used in Eq. (6) to obtain the eigenvalues and eigenfunctions.

Multifractal Formalism

Fractal modeling of turbulence was initiated by Mandelbrot[21] in his seminal paper on intermittent turbulence in self-similar cascades. Previously it had been thought that the logarithm of the dissipation would satisfy a Gaussian distribution. The distribution is then referred to as "lognormal." The term "micro-canonical" (Ref. 26) was used to describe conditions where the energy of all subeddies was conserved, whereas Mandelbrot's model was canonical, which represented energy distributions to the daughter eddies that were statistically independent and conserved only on the average.

It was found that a single fractal dimension D, which explained the growth rate of daughter eddies of the form 2^D, was not enough to describe the self-similar nature of turbulence. The multifractal formalism was born out of such a need. Multifractals are not sets. They are properly defined as measures in probabilistic terms. There are two methods of quantifying the concepts of multifractals: 1) the D_q vs q model (generalized fractal dimensions), and 2) the $f(\alpha)$ vs α model (the multifractal spectrum).

The generalized dimensions D_q are defined to be the scaling exponents for the qth moments of the measure. The (D_q,q) model was first formalized by Hentschel and Procaccia[27] in the context of dynamical systems. The $f(\alpha)$ spectrum has been related to the characterization of strange attractors of several well-known chaotic systems by Halsey et al.[28] The passage from $f(\alpha)$ to D_q and vice versa is obtained by an inverse or direct Legendre transformation. An excellent exposition by Mandelbrot[23] shows the connection to the Gibbs distribution in thermodynamics where α takes on the role of the Lagrange multipliers. The Lagrange multipliers are standard tools in minimizing cost functions with constraints and do not explicitly manifest themselves either in the (D_q,q) or $(f(\alpha),\alpha)$ curves.

The (D_q,q) quantities are direct extensions of the Hausdorff dimension definitions. Hausdorff measures are defined by

$$\sum_{\delta\to 0}^{i} \delta_i^d$$

where δ_i is the width of the covers (bins) and $\delta = \max\{\delta_i\}$. The Hausdorff dimension D is defined as

$$\sum_{\delta=0}^{i} \delta_i^d = \begin{cases} \infty & \text{for } d < D \\ 0 & \text{for } d > D \end{cases} \tag{10}$$

Likewise, (see Ref. 27 for details), one can extend the concept of Hausdorff measures by defining multifractal measures as

$$\sum_{i=1}^{N_\delta} p_i^q / \delta_i^\tau$$

where p_i is the probability of hitting the ith bin (cover) and N_δ is the number of nonempty bins. Similar to the jump at $d = D$,

$$\sum_{\delta=0}^{i} \frac{p_i^q}{\delta_i^\tau} = \begin{cases} \infty & \text{for } \tau > (q-1)D_q \\ 0 & \text{for } \tau < (q-1)D_q \end{cases} \tag{11}$$

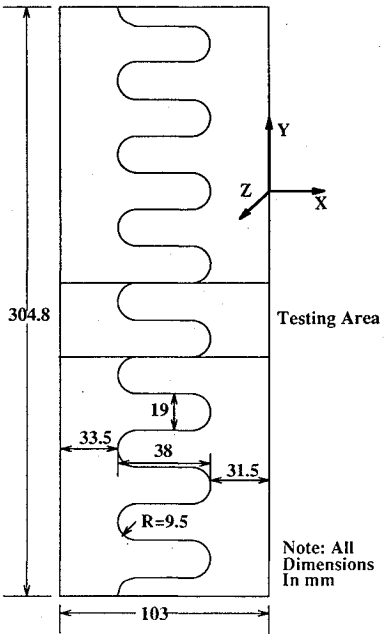

Fig. 3 Test section.

The generalized fractal dimensions are therefore defined as

$$D_q = \frac{\log\left(\sum_{i=1}^{N_\delta} p_i^q\right)}{(q-1)\log\delta} \tag{12}$$

where all δ_i have the same value δ, and N_δ is the smallest number of bins needed to cover the data. The quantity q refers to the qth moment of the invariant probability density function p_i. There are, of course, several difficult theoretical issues that determine whether these are indeed invariant probability measures. We will present several open questions dealing with convergence issues in the course of this presentation. Certain well-known quantities are byproducts of the definition in Eq. (12).

For $q=0$,

$$D_0 = \frac{\log N_\delta}{\log(1/\delta)} \tag{13}$$

one obtains the box dimension.

For $q=1$,

$$D_1 = \frac{-\sum p_i \log p_i}{\log\delta} \tag{14}$$

which is the information dimension or entropy.

Similarly, for $q=2$,

$$D_2 = \frac{\log\left(\sum_{i=1}^{N_\delta} p_i^2\right)}{\log\delta} \tag{15}$$

which is the correlation dimension.

The main differences between fractal sets and multifractal measures is that a fractal dimension is used to model geometric objects that exhibit self-similarity by one number, whereas the theory of multifractals is used to characterize a more complicated ensemble of data that is composed of interwoven sets of singularities of different strengths. The singularity strengths are defined by $p_i \approx \delta^\alpha$ and the number of times α takes on a value between α and $\alpha+d\alpha$ is of the form $\rho(\alpha)\delta^{-f(\alpha)}d\alpha$, where $f(\alpha)$ is a continuous function. The multifractal formalism therefore defines the different singularity strengths by α and each is characterized by its own fractal dimension $f(\alpha)$. The $f(\alpha)$ curve reflects the multifractal formalism better than the D_q computation because the $f(\alpha)$ vs α curve resembles a limit log-normal distribution in a region near the maximum $f(\alpha)$ value. The maximum value corresponds to $q=0$ and the analogy to the log-normal distribution can be rigorously shown by certain renormalization arguments.

It is important here to note that the term "dimension" is somewhat inappropriate in defining these quantities as they have some but not all of the properties of dimension. This is especially true when one considers low-dimensional cuts through high-dimensional multifractals (Ref. 29) as in the context of modeling turbulent flow. In this paper, we will review different methods of computing $f(\alpha)$ both indirectly (via the Legendre transformation from the D_q, which is computationally easier) and by the direct measurement from the scaling of histograms. The Legendre transformations are given by

$$\tau = (q-1)D_q \tag{16}$$

$$\alpha = \frac{d\tau}{dq} \tag{17}$$

$$f(\alpha) = \alpha q - \tau \tag{18}$$

The inverse transformation is given by

$$q = \frac{df(\alpha)}{d\alpha} \tag{19}$$

$$D_q = \frac{\alpha q - f(\alpha)}{q-1} \tag{20}$$

Meneveau and Sreenivasan[29] allude to the important observation that the intermediate step involving D_q involves smoothing of the data, which may have consequences that have not yet been fully understood.

To compute the $f(\alpha)$ spectrum directly, we use a method originally outlined by Mandelbrot[30] and later adopted by Chhabra and Jensen.[24] Define the quantity μ_i *as*

$$\mu_i = \frac{p_i}{\sum_j p_j^q} \tag{21}$$

By the thermodynamic analogy to entropy S, which is

$$S = -\sum_i p_i \log(p_i) \tag{22}$$

the singularity strength α can be written as

$$\alpha = \frac{\sum_i \mu_i \log(p_i)}{\log\delta} \tag{23}$$

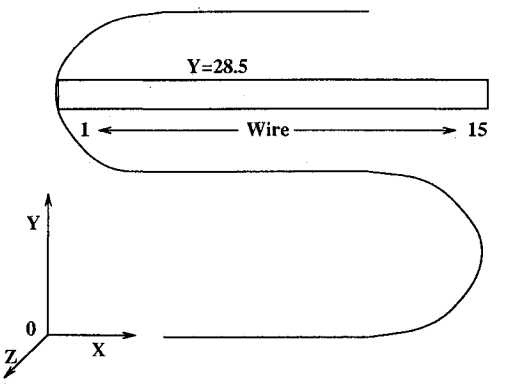

Fig. 4 Rake position.

Similarly,

$$f(\alpha)=\frac{\sum_i \mu_i \log(\mu_i)}{\log \delta} \tag{24}$$

Thus, we can directly determine both the D_q and the $f(\alpha)$ curves. We overlay the graphs obtained from direct methods over the curves computed via the Legendre transformation pair. Chhabra and Jensen[24] have noted that indirect methods for determining the $f(\alpha)$ curve have a propensity for undershooting or overshooting near D_0. The region near D_0 represents the top of the bell-shaped $f(\alpha)$ curve. For some of the hot-wire probes, however, it is observed that there is no visible undershoot or overshoot. We also document values of $f(\alpha)$ that are negative. By definition, $N(\alpha)=\delta^{-f(\alpha)}$, where $N(\alpha)$ is the number of bins that have scaling exponent α. Therefore, $f(\alpha)=\log[N(\alpha)]/\log(1/\delta)$. Since $\delta<1$, $\log(1/\delta)>0$. In order for $f(\alpha)<0$, $N(\alpha)$ must be less than 1. This seems impossible because $N(\alpha)$ is either zero or a positive integer. $N(\alpha)$ can only be less than 1 if large sample records are obtained and averaged to yield a fraction. If $f(\alpha)$ was a fractal dimension, this could not be true. Mandelbrot[30] replaces $f(\alpha)$ with the quantity

$$f(\alpha)=\rho(\alpha)-d \tag{25}$$

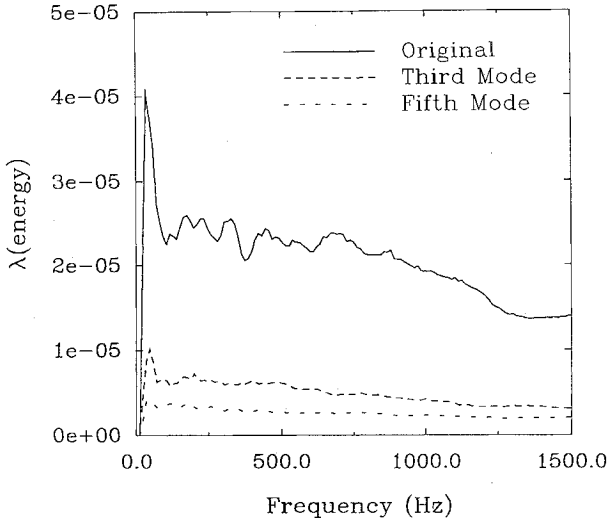

Fig. 5 Streamwise energy contained in the eigenspectral modes.

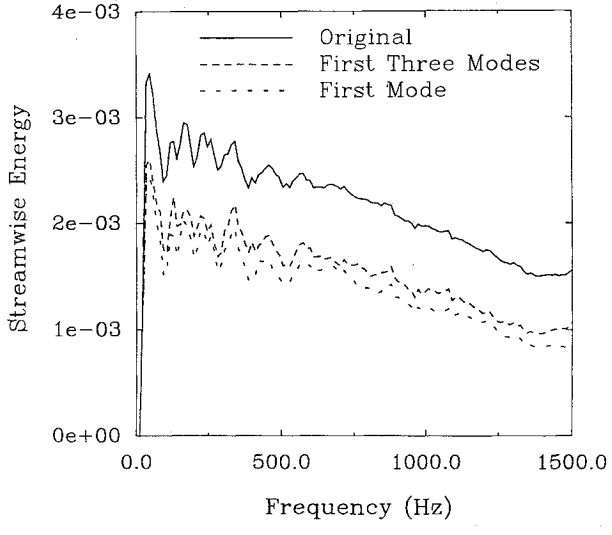

Fig. 6 Convergence of streamwise power spectra, wire 11.

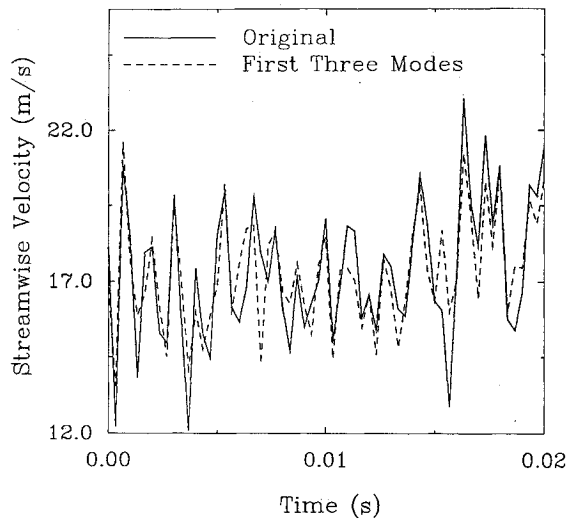

Fig. 7 Contribution from first three eigenmodes superimposed on the original instantaneous velocity time trace, wire 11.

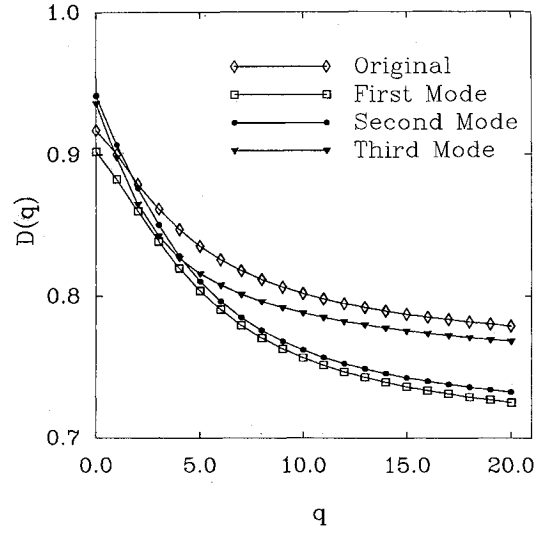

Fig. 8 $D(q)$ vs q, wire 5.

where d denotes the embedding dimension. Negative $f(\alpha)$ can therefore be interpreted as a consequence of taking lower-dimensional cuts cuts through higher-dimensional measures.

The intermittency exponent μ, computed based on the $f(\alpha)$ curves is

$$\mu=2[\alpha-1+d-f(\alpha)] \tag{26}$$

where d is the embedding dimension (in our case $d=1$) evaluated at $q=0$. Prasad et al.[31] have shown that stronger singularities correspond to greater values of μ; thus, curves with higher intermittency values are expected to flatten out at a slower rate.

Experiment and Apparatus

An illustration of the wind tunnel used in this study can be seen in Fig. 2. The tunnel was divided in half by a steel center plate. There was a 3-hp centrifugal blower coupled to a variable speed controller on both sides of the plate. The flow traveled through sections after leaving the blowers. The first section was a three-dimensional diffuser. The next section housed small mesh screens and a honeycomb filler for flow conditioning purposes. After this section, the flow traveled through a three-dimensional contraction section. The final section was the actual test section surrounding the lobed

Table 1 Intermittency values

Wire	Original	First mode	Second mode	Third mode
5	0.0204	0.0677	0.0776	0.1386
9	0.0498	0.0484	0.0326	0.0502
11	0.0758	0.0732	0.0669	0.0549
15	0.0015	0.0409	0.0232	0.0579

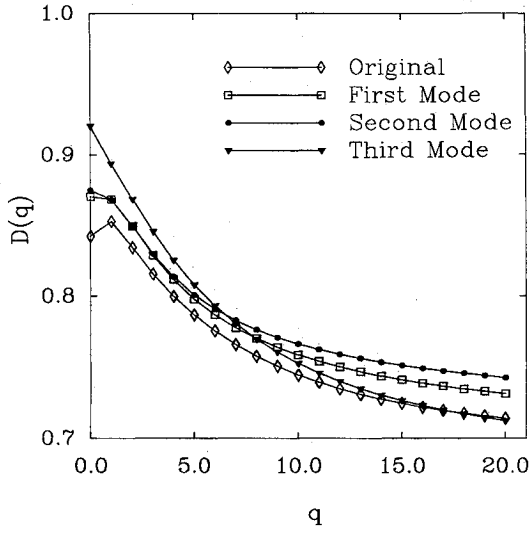

Fig. 9 $D(q)$ *vs* q, **wire 15.**

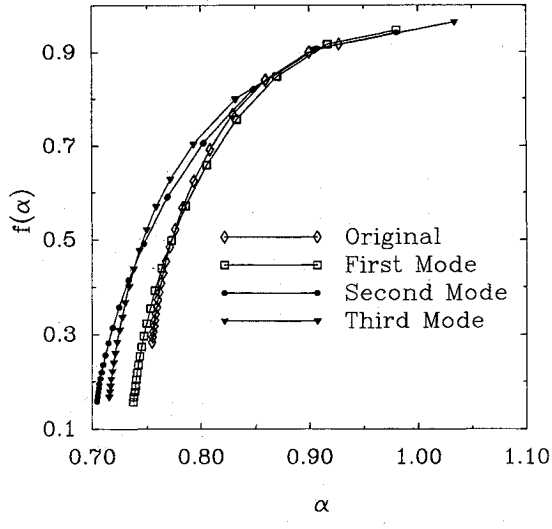

Fig. 10 $f(\alpha)$ **vs** α, **wire 5.**

mixer. A detailed front view of this section can be seen in Fig. 3. The lobed mixer was formed from a fiberglass flat plate and consisted of 15 full lobes with a penetration of 37.5%. The inlet conditions to the test section were documented by Eckerle et al.[3] They found the boundary layers on the plate leading to the lobe to be turbulent, whereas the core flow had a turbulence intensity of approximately 1%.

The streamwise velocity measurements were taken in the downstream region of the lobed mixer through the use of a specially designed rake of hot wires.[32] The rake consisted of 15 single component probes, with a tungsten sensing wire, spanning across a full lobe width spaced by 2.714 mm. For the data collection, a velocity ratio of 2:1 was used. Figure 4 shows the position of the rake in the testing area. The data was collected through the use of a Zenith 248 computer, a MetraByte DAS-20 12-bit analog/digital converter, and four MetraByte SSH-4 simultaneous sample and hold boards. All data were sampled at a rate of 3 kHz with a low-pass antialiasing filter set at 1.4 kHz. To ensure an adequate statistical sample, 100 blocks of 256 samples were taken. The hot wires were calibrated using a polynomial scheme as detailed by George et al.[33]

Results

The results from the application of the POD show the existence of a coherent structure or dominant eddy that contains a dominant part of the energy. The analysis for this study was done at several locations but we have only presented the data from one spatial location, 100 mm downstream at $y = 28.5$ (see Fig. 4). The total streamwise energy contained in the first, third, and fifth modes of the eigenspectra are shown in Fig. 5. The first eigenspectra contained 42% of the turbulent kinetic energy in the streamwise direction. The second and third modes combined contained another 28% of this energy. Figure 6 shows the original streamwise velocity power spectrum along with the first and sum of the first three modes for wire 11. This plot shows a noticeably quick convergence; if the spectrum from a location with lower energy was shown, the convergence would not be as quick. A comparison of the original streamwise velocity time trace to a reconstructed time trace using the first three eigenmodes is shown in Fig. 7 for wire 11. With only three modes, most of the characteristics of

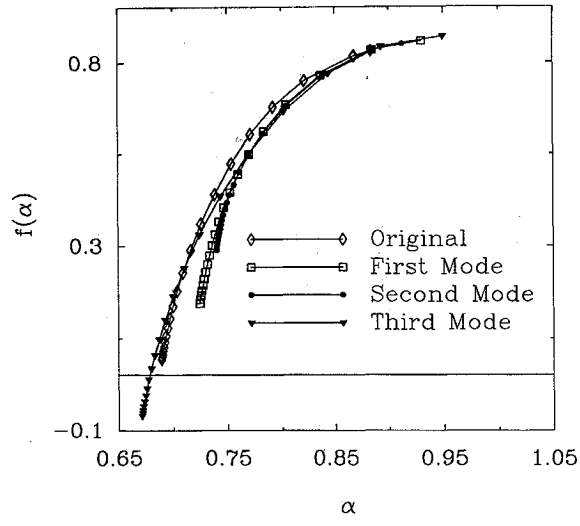

Fig. 11 $f(\alpha)$ **vs** α, **wire 15.**

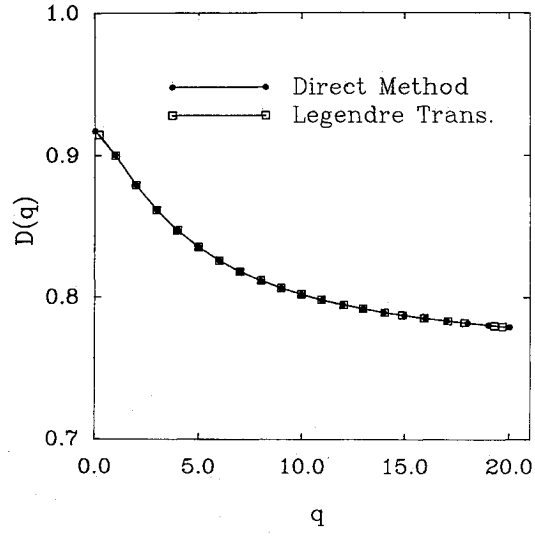

Fig. 12 D_q **vs** q **direct calculation compared to Legendre transformation, wire 5.**

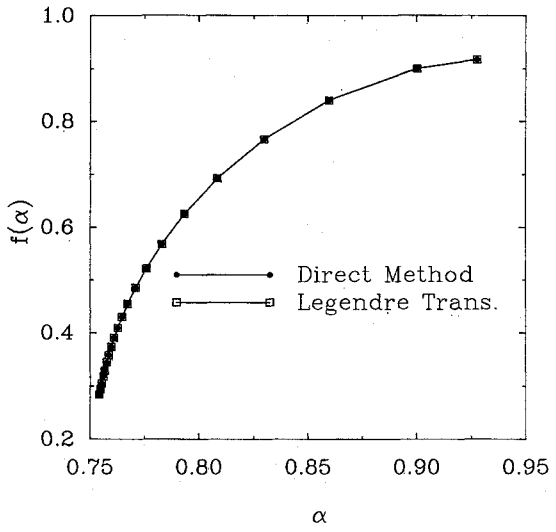

Fig. 13 $f(\alpha)$ vs α direct calculation compared to Legendre transformation, wire 5.

the original signal are represented (see Ref. 34), implying that this representation can be used to develop a low-dimensional dynamical systems model for the lobed mixer similar to the boundary-layer studies of Aubry et al.[35] and the axisymmetric jet studies of Glauser et al.[36]

Figures 8 and 9 show D_q,q curves, which were calculated, using the direct method, from the data taken for wires 5 and 15. The values of (D_q,q) were calculated using the original signal and the reconstructed signals using the first, second, and third eigenmodes. Figure 8 represents a spatial location with higher turbulent energy, whereas Fig. 9 shows a location of lower turbulent energy in the flowfield. These two figures show that at locations with lower energy content the curves flattened out quicker (for the original signal), implying that more information was contained in D_1. More significantly, these locations also corresponded to lower values of intermittency, as seen in Table 1 (Table 1 also shows intermittency values for wire 9 and 11). From this and looking at the curves for the various eigenmodes, it is apparent that the lower the intermittency value the faster the curve flattens out.

We report here previously undocumented characteristics of the multifractal spectrum of reconstructed time traces from application of the POD. Figures 10 and 11 show $(f(\alpha),\alpha)$ curves that were calculated directly in the method described by Chhabra and Jensen.[24] Similar to the (D_q,q) curves, these graphs also vary directly with the values of intermittency. By examining the curves calculated from the measured time traces, it is apparent that the locations with a corresponding higher intermittency value are spread out farther along the α axis. This relationship can also be noticed by examining the $(f(\alpha),\alpha)$ curves calculated from the reconstructed time traces of the various modes.

Figures 12 and 13 show a comparison of direct calculations for $(f(\alpha)\alpha)$ and (D_q,q). These graphs show good agreement whether we used the forward or inverse Legendre transformation.

It is important to note that even if the original velocity time trace exhibits low intermittency, the signals reconstructed from the POD for individual modes can show significant multifractal character. For example, see the results in Table 1 for wire number 5.

Conclusions

The quantities D_q, which have been computed for positive q for the first three eigenmodes using the POD, reflect the scaling structure of the flowfield. Although the (D_q,q) method does not replace spectral analysis, it can be used to locate areas of high turbulent energy in the flowfield in an alternative manner that appeals to the intuitive notion of self-similarity. Moreover the $(f(\alpha),\alpha)$ curves obtained through direct and indirect methods have been shown to exhibit no discontinuities [discontinuities in the $f(\alpha)$ spectrum are symptomatic of phase transitions]. In general, the third mode exhibits a greater multifractal character than the original signal and the first and second modes. One can possibly infer from this that the higher proper orthogonal modes correspond to smaller scales in the flowfield, which is consistent with the pseudo flow visualization results of Ukeiley et al.[34]

Acknowledgment

This work was completed with support from the Cornell-Clarkson NASA Space Grant Consortia. This source of support is gratefully acknowledged.

References

[1]Paterson, R. W., "Turbofan Mixer Nozzle Flowfield—A Benchmark Experimental Study," *Journal of Engineering for Gas Turbines and Power*, Vol. 106, 1982, pp. 692–698.

[2]Werle, M. J., Presz, W., and Paterson, R. W., "Flow Structure in a Periodic Axial Vortex Array," AIAA Paper 87-0160, Jan. 1987.

[3]Eckerle, W. A., Sheibani, H., and Awad, J., "Experimental Measurements of the Vortex Development Downstream of a Lobed Forced Mixer," American Society of Mechanical Engineers, Paper 90-GT-27, June 1990.

[4]Lasheras, J. C., and Meiburg, E., "Three-Dimensional Vorticity Modes in the Wake of a Flat Plate," *Physics of Fluids A*, Vol. 2, No. 3, 1990, pp. 371–380.

[5]Lumley, J. L., "The Structure of Inhomogeneous Turbulent Flows," *Atmospheric Turbulence and Radio Wave Propagation*, edited by A. M. Yaglom and V. I. Tartarsky, Nauka, Moscow, 1967, pp. 166–178.

[6]Loeve, M., *Probability Theory*, Van Nostrand, Princeton, NJ, 1955.

[7]Payne, F. R., "Large Eddy Structure of a Turbulent Wake," Ph.D. Dissertation, Pennsylvania State Univ., Dept. of Aerospace Engineering, University Park, PA, Sept. 1966.

[8]Bakewell, P., and Lumley, J. L., "Viscous Sublayer and Adjacent Wall Region in Turbulent Pipe Flow," *Physics of Fluids*, Vol. 10, No. 9, 1967, pp. 1880–1889.

[9]Moin, P., "Probing Turbulence via Large Eddy Simulation," AIAA Paper 84-0174, Jan. 1984.

[10]Herzog, S., "The Large Scale Structure in the Near-Wall of Turbulent Pipe Flow," Ph.D. Dissertation, Cornell Univ., Dept. of Mechanical and Aerospace Engineering, Ithaca, NY, Jan. 1986.

[11]Leib, S. J., Glauser, M. N., and George, W. K., "An Application of Lumley's Orthogonal Decomposition to the Axisymmetric Jet Mixing Layer, " *Proceedings of the 9th Rolla Symposium*, Univ. of Missouri at Rolla, Rolla, MO, 1984.

[12]Glauser, M. N., Leib, S. J., and George, W. K., "Coherent Structures in the Axisymmetric Jet Mixing Layer," *Turbulent Shear Flows 5*, Springer-Verlag, Germany, 1987, pp. 134–145.

[13]Glauser, M. N., and George, W. K., "An Orghogonal Decomposition of the Axisymmetric Jet Mixing Layer Utilizing Cross-Wire Measurements," *Proceedings of Turbulent Shear Flows 6*, Toulouse, France, 1987, pp. 10.1.1–10.1.6.

[14]Sirovich, L., Maxey, M., and Tarman, H., "Analysis of Turbulent Thermal Convection," *Proceedings of Turbulent Shear Flows 6*, Toulouse, France, 1987, pp. 12.5.1–12.5.6.

[15]Chambers, D. H., Adrian, R. J., Moin, P., Stewart, D. S., and Sung, H. J., "Karhunen-Loeve Expansion of Burgers' Model of Turbulence," *Physics of Fluids*, Vol. 31, No. 9, 1988, pp. 2573–2582.

[16]Delville, J., Bellin, S., and Bonnet, J. P., "Use of the Proper Orthogonal Decomposition a Plane Turbulent Mixing Layer," *Turbulence and Coherent Structures*, edited by O. Metais and M. Lesieur, Kluwer, The Netherlands, 1991, pp. 75–91.

[17]Sirovich, L., Kirby, M., and Winter, M., "An Eigenfunction Approach to Large Scale Transitional Structures in Jet Flow," *Physics of Fluids A*, Vol. 2, No. 2, 1991, pp. 127–136.

[18]Winter, M., Barber, T. J., Eerson, R., and Sirovich, L., "Eigenfunction Analysis of Turbulent Mixing Phenomenon," AIAA Paper 91-0520, Jan. 1991.

[19]Kolmogorov, A. N., "A Refinement of Previous Hypotheses Concerning the Local Structure of Turbulence in a Viscous Incompressible Fluid at High Reynolds Number," *Journal of Fluid Mechan-*

ics, Vol. 13, 1962, pp. 82–85.

[20]Mandelbrot, B. B., "Possible Refinement of the Lognormal Hypothesis Concerning the Distribution of Energy Dissipation in Intermittent Turbulence," *Statistical Models and Turbulence*, edited by M. Rosenblatt and C. W. Van Atta, Springer, 1972, pp. 333–351.

[21]Mandelbrot, B. B., "Intermittent Turbulence in Self-Similar Cascades: Divergence of High Moments and Dimension of the Carrier, *Journal of Fluid Mechanics*, Vol. 62, 1974, pp. 331–358.

[22]Meneveau, C., and Sreenivasan, K. R., "Simple Multifractal Cascade Model for Fully Developed Turbulence," *Physical Review Letters*, Vol. 59, No. 13, 1987, pp. 1424–1427.

[23]Mandelbrot, B. B., "Multifractal Measures, Especially for the Geophysicist," *Pure and Applied Geophysics*, Vol. 131, 1989, pp. 5–42.

[24]Chhabra, A., and Jensen, R. V., "Direct Determination of the $f(\alpha)$ Singularity Spectrum," *Physical Review Letters*, Vol. 62, No. 12, 1989, pp. 1327–1330.

[25]Moin, P., and Moser, R. D., "Characteristic-Eddy Decomposition of Turbulence in a Channel," *Journal of Fluid Mechanics*, Vol. 200 1989, pp. 471–509.

[26]Yaglom, A. M., "The Influence of the Fluctuation in Energy Dissipation on the Shape of Turbulent Characteristics in the Inertial Interval," *Dokl. Akad. Nauka SSSR*, Vol. 166, 1962, pp. 49–52. (English Trans. So. Phys. Dokl. No. 2, pp. 26–29).

[27]Hentschel, H. G. E., and Procaccia, I., "The Infinite Number of Generalized Dimensions of Fractals and Strange Attractions," *Physica D*, Vol. 8, 1983, pp. 435–444.

[28]Halsey, T. C., Jensen, M. H., Kadanoff, L. P., Procaccia, I., and Sharaiman, B. I., "Fractal Measures and Their Singularities: The Characterization of Strange Sets," *Physical Review A: General Physics*, Vol. 33, No. 2, 1986, p. 1141.

[29]Meneveau, C., and Sreenivasan, K. R., "Measurement of $f(\alpha)$ From Scaling of Histograms and Applications to Dynamical Systems and Fully Developed Turbulence," *Physics Letters A*, Vol. 137, No. 3, 1989, pp. 103–112.

[30]Mandelbrot, B. B., "Multifractals in Geophysics," *Fluctuations and Pattern Formation Cargeses*, edited by H. E. Stanley and N. Ostrowsky, Kluwer, Dordrecht, The Netherlands, 1988.

[31]Prasad, R. R., Meneveau, C., and Sreenivasan, K. R., "Multifractal Nature of the Dissipation Field of Passive Scalars in Fully Turbulent Flows," *Physical Review Letters*, Vol. 61, No. 1, 1988, pp. 74–77.

[32]Ukeiley, L., Wick, D., and Glauser, M., "A Novel Hot-Wire Rake Design," ASME FED, Vol. 97, 1990, pp. 87–92.

[33]George, W. K., Beuther, P. D., and Shabbir, A., "Polynomial Calibrations for Hot Wires in Thermally-Varying Flow," ASME FED Vol. 53, 1987, pp. 3–6.

[34]Ukeiley, L., Wick, D., and Glauser, M., "Coherent Structure Identification in a Lobed Mixer," American Society of Mechanical Engineers, Paper 91-GT-397, June 1991.

[35]Aubry, N., Holmes, P., Lumley, J. L., and Stone, E., "The Dynamics of Coherent Structures in the Wall Region of a Turbulent Boundary Layer," *Journal of Fluid Mechanics*, Vol. 192, 1988, pp. 115–173.

[36]Glauser, M. N., Zheng, X., and Doering, C. R., "The Dynamics of Organized Structures in the Axisymmetric Jet Mixing Layer, *Turbulence and Coherent Structures*, edited by O. Metais and M. Lesieur, Kluwer, The Netherlands, 1991, pp. 253–266.